11-1-2017

Evaluation of WRF SCM Simulations of Stratocumulus-Topped Marine and Coastal Boundary Layers and Improvements to Turbulence and Entrainment Parameterizations

Mohamed S. Ghonima
University of California, San Diego

Handa Yang
University of California, San Diego, hay022@ucsd.edu

Chang Ki Kim
Korea Institute of Energy Research

Thijs Heus
Cleveland State University, t.heus@csuohio.edu

Jan Kleissl
University of California, San Diego

AGU PUBLICATIONS

Journal of Advances in Modeling Earth Systems

RESEARCH ARTICLE
10.1002/2017MS001092

Key Points:
- The modeling of stratocumulus-topped boundary layers over both land and ocean in numerical weather prediction models is analyzed
- The consistent cold, moist bias over four different test cases indicates a lack of entrainment mixing
- Proposed changes to improve simulations include mixing caused by cloud top cooling and explicit entrainment modeling, with good results

Correspondence to:
H. Yang,
hay022@ucsd.edu

Citation:
Ghonima, M. S., Yang, H., Kim, C. K., Heus, T., & Kleissl, J. (2017). Evaluation of WRF SCM simulations of stratocumulus-topped marine and coastal boundary layers and improvements to turbulence and entrainment parameterizations. *Journal of Advances in Modeling Earth Systems*, *9*, 2635–2653. https://doi.org/10.1002/2017MS001092

Received 22 JUN 2017
Accepted 23 OCT 2017
Accepted article online 27 OCT 2017
Published online 17 NOV 2017

Evaluation of WRF SCM Simulations of Stratocumulus-Topped Marine and Coastal Boundary Layers and Improvements to Turbulence and Entrainment Parameterizations

Mohamed S. Ghonima[1], Handa Yang[1], Chang Ki Kim[2], Thijs Heus[3], and Jan Kleissl[1]

[1]Center for Renewable Resources and Integration, Department of Mechanical and Aerospace Engineering, University of California, San Diego, La Jolla, CA, USA, [2]New and Renewable Energy Resource Center, Korea Institute of Energy Research, Yuseong-gu, Daejeon, Korea, [3]Department of Physics, Cleveland State University, Cleveland, OH, USA

Abstract Stratocumulus-topped boundary layers (STBLs) are notoriously difficult to parameterize in single-column models due to the strong inversion layer across which entrainment mixing plays an important role in modulating the boundary layer mass, energy, and moisture balances. We compare three different WRF planetary boundary layer (PBL) schemes (Yonsei University, YSU; Asymmetric Convective Model version 2, ACM2; Mellor-Yamada-Nakanishi-Niino, MYNN) against large eddy simulations (LES) to find out that they underestimate entrainment flux in stratocumulus over both ocean and coastal land. Hence, the PBL schemes produce a cooler, moister STBL with higher liquid water content. In order to improve the entrainment parameterization, we propose a modification to the YSU scheme that takes into account the in-cloud turbulence flux contribution to cloud top entrainment through the formulation of a velocity scale based on the in-cloud buoyancy flux. A revised top-down mixing profile is also implemented to model mixing due to turbulence generated by longwave cooling at the cloud top. The modified YSU simulates stronger entrainment flux, resulting in a STBL that matches LES results. Similar modifications were made to ACM2 in addition to implementing explicit entrainment, and while the results also showed good agreement with LES, discretization issues and conflicts with its original design prevent immediate implementation, as the contribution from the modifications and the original scheme are difficult to correctly modulate.

Plain Language Summary This study evaluates the simulation of common low-level clouds in numerical weather prediction models. The model of interest simulates air masses which are too cold and moist. Modifications were made to increase mixing of air between the cloud top and the land surface, as well as to more accurately simulate the small-scale mixing at the cloud top interface. Results were compared against a more accurate, higher resolution model, and were found to be more accurate. These improvements may aid the weather forecasting community through heat and humidity prediction, the aviation industry through cloud ceiling height prediction, as well as the solar energy and climate modeling communities through cloud cover prediction.

1. Introduction

Stratocumulus clouds are a common occurrence across the globe and have a strong impact on the local boundary layer energy and water budgets as well as the global climate (Hahn & Warren, 2007; Hartmann & Short, 1980; Randall et al., 1984). Stratocumulus clouds usually form under a sharp inversion that may only be a few meters thick. Because of the large range of spatial scales and turbulent motions associated with stratocumulus clouds and the limited resolution of models, numerical weather prediction (NWP) and global climate models (GCMs) parameterize the turbulence within the boundary layer through planetary boundary layer (PBL) schemes. Of particular importance to stratocumulus is entrainment (mixing) across the inversion, which is driven by turbulence generated in the boundary layer through cloud top longwave and evaporative cooling, thus entrainment plays an integral role in determining the liquid water path (LWP), lifetime, and spatial extent and structure of the clouds (Ghonima et al., 2016; Moeng, 2000). However, the mixing processes occurring near the cloud top between the two-phase fluids at very high Reynolds numbers have proven difficult to address even with the highest resolution models (Stevens, 2010). As this process is better

understood, new parameterization methods are being developed to more accurately represent its impact on the stratocumulus-topped boundary layer (STBL) and its breakup. Efforts to develop physical models of stratocumulus have traditionally been focused on idealized marine cases, with stratocumulus clouds over land receiving less attention; however, stratocumulus clouds impact agriculture, solar installations, and aviation visibility, for example. We therefore extend stratocumulus test cases to land as well as over ocean conditions.

In contrast to NWPs and GCMs, large eddy simulations (LES) have higher resolutions and are able to explicitly represent the energetic larger turbulent eddies within the boundary layer while the smaller eddies are parameterized. Multiple intercomparison studies of LES of STBL have found good agreement with measurements from various field campaigns (Ackerman et al., 2009; Stevens et al., 2005). Hence, LES have been utilized as benchmarks to evaluate different PBL schemes. Comparing against LES and measurements from the DYCOMS campaign, Zhu et al. (2005) evaluated the capability of 10 single-column models (SCMs) to model the STBL and found that although all models were capable of maintaining the sharp inversion, liquid water paths (LWP) varied by a factor of 10 between SCMs.

To identify the cause of this discrepancy and improve the representation of STBL in NWPs and GCMs, in this paper we employ the findings of Ghonima et al. (2016), where an improved parameterization for cloud top entrainment mixing in a mixed layer model improved simulations of both coastal and marine stratocumulus. We evaluate several SCM representations of the STBL in the Weather Research and Forecasting (WRF; Skamarock et al., 2008) model against LES. Due to its importance, a specific focus is the SCM representation of entrainment or mixing across the inversion. We analyze the Yonsei University (YSU) scheme that is a first-order scheme that models flux as a function of the eddy viscosity (Hong et al., 2006). The model includes a correction for counter-gradient mixing and explicitly models the entrainment at the inversion. YSU was recently updated with a top-down mixing model and a revision to the entrainment model to better simulate fog (Wilson, 2015). Second, we investigate the Asymmetric Convective Model version 2 (ACM2) that is also a first-order scheme but uses a transilient matrix that defines mass flux to account for the convective eddies instead of using a counter-gradient correction term (Pleim, 2007). Finally, we examine the Mellor-Yamada-Nakanishi-Niino (MYNN) model, which is a turbulent kinetic energy (TKE) closure scheme (Nakanishi & Niino, 2004). MYNN uses TKE, which in theory provides a better measure of turbulence in the STBL, to determine the eddy diffusivity. Both the YSU and the ACM2 are less complex, more computationally economical models while the MYNN scheme takes into account more of the physics of the boundary layer at a higher computational cost.

To account for the effects of the microphysics parameterizations, we run each PBL scheme with four different microphysics schemes offered in WRF. In section 3, we find that (with the exception of the recent Wilson (2015) update to YSU) the above PBL models are unable to account for the turbulence generated by cloud top longwave cooling and therefore underestimate entrainment flux. We propose a correction to the velocity scale in the YSU PBL parameterization based on the in-cloud buoyancy flux in order to improve the representation of longwave-generated cooling. Simulations of both coastal (under dry and moist land surface conditions) and marine (with two different initial profiles) STBL through an entire 24 h diurnal cycle resulted in better agreement with the LES (section 4). In conclusion, section 5 provides a discussion on the ability of the changes introduced here to address the deficiencies in current PBL schemes and improve the simulation of STBL over coastal lands and ocean.

2. Design of Numerical Experiments

2.1. Model Setup

For this analysis, we used WRF v3.7.1 in single-column mode to evaluate three PBL and four microphysics schemes (refer to Tables 1 and 2 for an overview of the schemes). The vertical domain of the SCM consists of 74 levels up to an altitude of 10,000 m (with 49 levels concentrated below 2 km), and the simulation time step is 20 s. The SCM employs the New Goddard scheme for longwave and shortwave radiation (Chou & Suarez, 1999, 2001), Monin-Obukhov similarity theory for the surface layer parameterization (Paulson, 1970), and the Kessler microphysics scheme (Kessler, 1969). The radiation scheme is called at every time step. For conciseness, we do not examine the impact of radiative, surface, and land parameterizations (surface fluxes are assumed constant in ocean cases) and instead focus on the fluxes into or out of the boundary layer at

Table 1
List of PBL Schemes Used in This Study

PBL scheme	Parameterization type	Reference
Yonsei University (YSU)	First-order closure scheme. Turbulence is parameterized using the eddy-diffusivity approach and a gradient adjustment term is added to account for large-scale eddies. Entrainment is explicitly modeled.	Hong et al. (2006)
Asymmetric convective Model version 2 (ACM2)	First-order nonlocal closure scheme. Turbulence is parameterized as a combination of local eddy diffusion and a nonlocal transilient matrix that defines mass flux between any pair of model layers.	Pleim (2007)
Mellor-Yamada-Nakanishi-Niino level 2.5 (MYNN)	TKE closure scheme	Nakanishi and Niino (2004, 2009)

the land surface and across the inversion. As reference cases, we utilize the DYCOMS RF01 initial profile in agreement with the intercomparison study conducted by Zhu et al. (2005). Following Zhu et al. (2005), we set the surface sensible heat flux (SHF) to be 15 W m^{-2} and the latent heat flux (LHF) to be 115 W m^{-2} for the DYCOMS RF01 ocean case. Simulations of STBL over wet and dry coastal lands were also conducted using the DYCOMS RF01 initial profiles using a simplified land surface model as described in Ghonima et al. (2016) which was coupled to both the LES and SCM. Unlike in the DYCOMS SCM intercomparison study that evaluated a nocturnal 6 h simulation, we run a 24 h simulation in order to study how well the SCM is capable of simulating the STBL over the diurnal cycle that is driven by shortwave radiative absorption in the cloud deck. All simulations are initialized at midnight.

To demonstrate generalizability of the results, additional simulations are run on the CGILS S12 control initial profile, which is a well-mixed STBL that has been used to evaluate both LES and SCM (Blossey et al., 2013; Zhang et al., 2012, 2013). The SHF and LHF for the CGILS S12 control ocean case were 5 and 80 W m^{-2}, which were approximated by first running an LES simulation with modeled surface fluxes and then taking the approximate 24 h mean values. The LES results shown here were run with the subsequent fixed fluxes.

The UCLA-LES model is set up as in the DYCOMS LES intercomparison study (Stevens et al., 2005). The only difference is that we couple the LES to a one-dimensional radiative model with Monte Carlo sampling of the spectral integration rather than the parameterized radiative scheme employed in the DYCOMS LES intercomparison (Pincus & Stevens, 2009; Stevens et al., 2005). We find that the one-dimensional radiative model produces fluxes that are closer to the New Goddard scheme employed in the WRF SCM. Minimizing this source of discrepancy allows a focused validation of the PBL parameterization.

2.2. PBL Scheme Formulation

2.2.1. YSU

2.2.1.1. YSU: Model Description

Following Hong et al. (2006), the YSU scheme parameterizes the vertical turbulent flux $\overline{w'c'}$ of any prognostic variable C (where the overbar denotes an ensemble average and lowercase with primes denote deviations from the average, and W is the vertical wind speed) as

Table 2
List of Microphysics Schemes Used for the Microphysics Sensitivity Study

Microphysics scheme	Hydrometeors	Reference
Kessler	Water vapor, cloud water, rain	Kessler (1969)
Lin	Water vapor, cloud water, ice, rain, snow and graupel	Lin et al. (1983)
Thompson	Water vapor, cloud water, rain, ice, snow and graupel	Thompson et al. (2008)
WSM5	Water vapor, cloud water, rain, ice, and snow	Hong et al. (2004)

$$\left(\overline{w'c'}\right)_{YSU} = -K_C\left(\frac{\partial C}{\partial z} - \gamma_c\right) + \overline{w'c'}_{z_{inv}}\left(\frac{z}{z_{inv}}\right)^3. \quad (1)$$

With the newly added top-down mixing option (Wilson, 2015), YSU expresses the eddy-diffusivity coefficient K_c in cloud-capped boundary layers as a linear combination of surface-driven mixing and top-driven mixing:

$$K_c = \kappa w_s z(1 - z/z_{inv})^2 + \kappa w_{pbl}\left(\frac{z^2}{z_{inv}}\right)(1 - z/z_{inv}), \quad (2)$$

where κ is the von Karman constant, z is height, and z_{inv} is the inversion base height. The mixed-layer velocity scale is expressed as $w_s = \left(u_*^3 + \phi_{h,m} k w_{*b}^3 z/z_{inv}\right)^{1/3}$ where u_* is the surface friction velocity, $\phi_{h,m}$ is the wind profile function evaluated at the top of the surface layer, and $w_{*b} = \left[g/\theta_{va}\left(\left(\overline{w'\theta_v'}\right)_0 z_{inv}\right)\right]^{1/3}$ is the convective velocity scale. The surface-driven profile is zero at the surface and PBL top, with a maximum in the lower third of the boundary layer. The top-down velocity scale w_{pbl} is formulated in the same way as w_s except w_{pbl} is a function of the PBL top flux, so the top-driven profile maintains the same shape as the surface-driven profile but is reversed so the maximum occurs in the top third of the boundary layer.

In equation (1), γ_c is the counter-gradient term and incorporates the contributions of large-scale eddies to the total flux and is computed as $\gamma_c = b\frac{\left(\overline{w'c'}\right)_0 + \left(\overline{w'c'}\right)_{z_{inv}}}{w_{s0} z_{inv}}$, where $\left(\overline{w'c'}\right)_0$ represents the surface flux, $\left(\overline{w'c'}\right)_{z_{inv}} = w_e \Delta C_{z_{inv}}$ represents the PBL top flux, $\Delta C_{z_{inv}} = C_{z_{inv}+1} - C_{z_{inv}}$ represents the jump value of C across the inversion, and b is a coefficient of proportionality. Finally, entrainment w_e is parameterized as

$$w_e = -\frac{\theta_{v0}}{g\Delta\theta_{vi} z_{inv}}\left(0.15 w_m^3 + A w_T^3\right), \quad (3)$$

where A is computed following the integral closure method described by Grenier and Bretherton (2001) as $A = a_1(1 + a_2 E)$ with $a_1 = 0.2$ and $a_2 = 8$. Here $a_2 E$ describes the evaporative enhancement of entrainment. Typical values of A range from about 0.2 to 0.5 for the cases simulated here. Finally, θ_{v0} is the reference virtual potential temperature, $\Delta\theta_{vi}$ represents the inversion jump, w_m^3 is a velocity scale based on the surface turbulence,

$$w_m^3 = w_*^3 + 5u_*^3, \quad (4)$$

where $w_* = \left[g/\theta_{va}\left(\left(\overline{w'\theta'}\right)_0 z_{inv}\right)\right]^{1/3}$ is the mixed-layer velocity scale for dry air (when $\theta = \theta_v$), and $w_T = \left[g/\theta_{va}\left(\left(\overline{w'\theta'}\right)_{rad} z_{inv}\right)\right]^{1/3}$ is a velocity scale based on the net radiative flux divergence at the cloud top F_{rad} with $\left(\overline{w'\theta'}\right)_{rad} = \frac{F_{rad}}{\rho c_p}$.

2.2.1.2. Proposed Modifications: YSU-BUOY

The second term in equation (3) is intended to describe the contribution of cloud top longwave radiative cooling to turbulence generated in the STBL. These thermals originate at the cloud top and sink through the STBL, as shown in plots of the third moment of vertical wind speed (Figure 1c, later). Currently, the top-driven eddy-diffusivity profile in the YSU scheme (equation (2)) is simply a reversed version of the surface-driven profile without adjusting the shape. However, based on LES results, mixing is more intense near the source of turbulence (i.e., cloud top), so we revise the eddy-diffusivity profile following Lock et al. (2000) to capture the skewness in cloud top driven mixing, as

$$K_c = \kappa w_s z(1 - z/z_{inv})^2 + \kappa w_{cld}\left(\frac{z^2}{z_{inv}}\right)(1 - z/z_{inv})^{0.5}, \quad (5)$$

where w_{cld} is the cloud velocity scale and is formulated as

$$w_{cld} = \frac{g}{\theta_{v0}}\int_{z_b}^{z_{inv}} \overline{w'\theta_v'} dz, \quad (6)$$

with the cloud base height z_b taken as the lowest grid level with liquid water content. Note that the exponent in the quantity $\left(1 - \frac{z}{z_{inv}}\right)^p$ differs from equation (2) (where p is implied to be 1) here in equation (5)

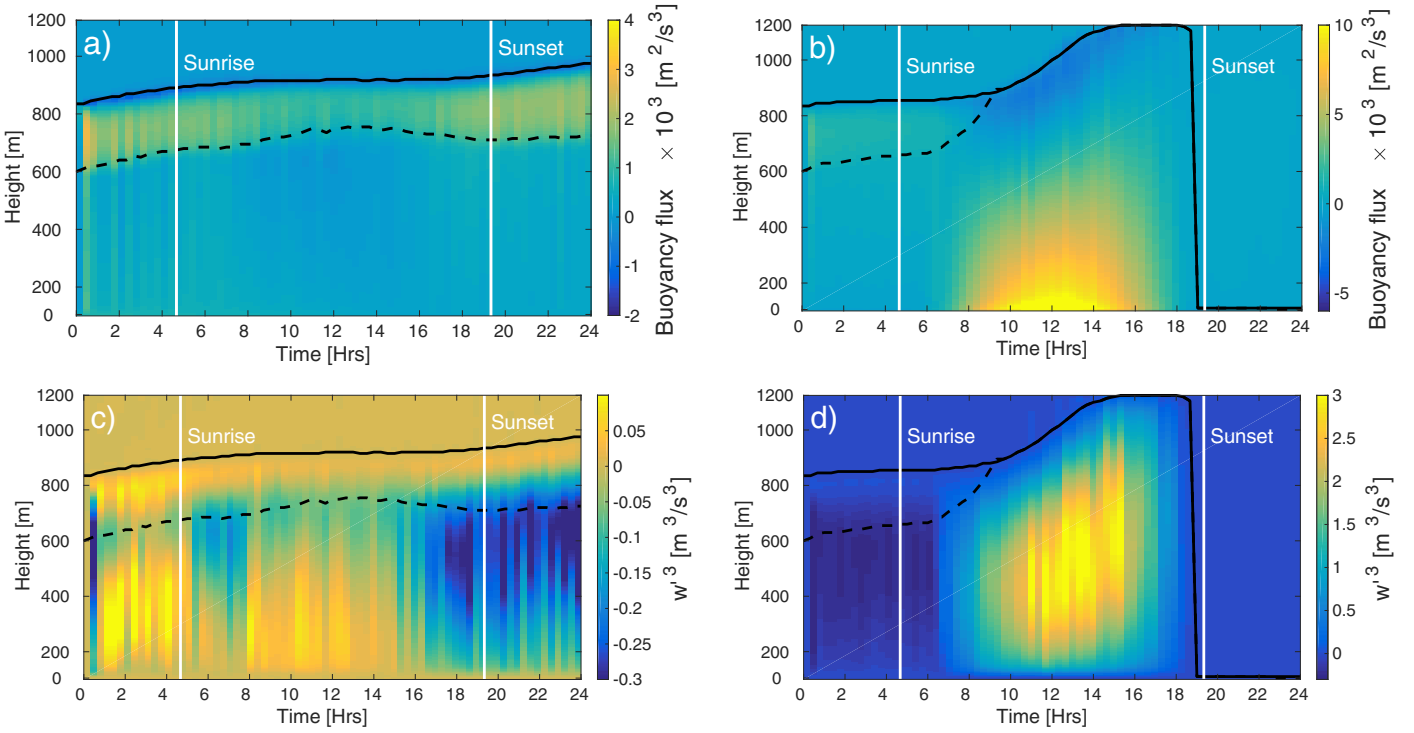

Figure 1. Horizontally averaged temporal evolutions from LES for the DYCOMS case of vertical profiles of (a, b) buoyancy flux and (c, d) third moment of vertical velocity ($\overline{w'^3}$). Results are shown for the DYCOMS RF01 ocean case (Figures 1a and 1c) and land case with Bowen ratio equal 1.0 (Figures 1b–1d). While the LES domain extends up to 1.6 km, only the lowest 1.2 km is shown to focus on the boundary layer dynamics. Inversion height is indicated by solid black lines, and cloud base by dashed black.

(p=0.5), though our tests have indicated negligible differences (not shown). The virtual potential temperature vertical flux is expressed as

$$\overline{w'\theta_v'}(z) = D_1\overline{w'\theta_l'}(z) + D_2\overline{w'q_T'}(z), \quad z_b < z < z_{inv}, \tag{7}$$

where $D_1 = \frac{1+\frac{\overline{q_s}}{\epsilon}-\overline{q_T}+\frac{\overline{\theta}}{\epsilon}\left(\frac{dq_s}{dT}\right)}{1+\frac{L_v}{c_p}\left(\frac{dq_s}{dT}\right)} \approx 0.5$ and $D_2 = \frac{L_v}{c_p}\left(\frac{1+\frac{\overline{q_s}}{\epsilon}-\overline{q_T}+\frac{\overline{\theta}}{\epsilon}\left(\frac{dq_s}{dT}\right)}{1+\frac{L_v}{c_p}\left(\frac{dq_s}{dT}\right)}\right) - \overline{\theta} \approx 970$ K within the cloud layer (see Stevens, 2002 for a more detailed derivation of the constants). Here these coefficients are treated as constants for computational efficiency. Instead of formulating the cloud velocity scale as function of radiative divergence (as in both Lock et al., 2000; Wilson, 2015), we have chosen the buoyancy flux within the cloud layer, as longwave emission becomes insensitive to LWP changes for thick clouds (LWP > 50 g m^{-2}; Kazil et al., 2015). Thus, by formulating w_{cld} as function of radiative divergence the parameterization fails to account for additional turbulence generated by latent heat releases in updrafts within in the cloud layer. Additionally, parameterizations dependent on the radiative flux divergence are bound to the frequency at which the radiative scheme is called, which may introduce further sensitivity and errors if the radiative time step is long.

Similarly, the entrainment velocity parameterization was revised to not be a function of radiative divergence. Hence, following Ghonima et al. (2016), we define a new velocity scale for the entrainment parameterization in equation (3) as

$$w_T^{*3} = 1.25\frac{gz_{inv}}{\theta_{v0}}\overline{w'\theta_v's} + 2.5\frac{g}{\theta_{v0}}\int_{z_b}^{z_{inv}}\overline{w'\theta_v'}dz. \tag{8}$$

The convective velocity scale in equation (8) follows Lock and Macvean (1999), except instead of using the net radiative flux we use the integral of the in-cloud buoyancy flux. For YSU-BUOY, we use the original closure constants of Nicholls and Turton (1986) in the computation of A in equation (3), so that a_2=60; typical values of A for the YSU-BUOY simulations ranged from about 0.5 to 0.9. Finally, the updated entrainment

parameterization uses only the second term in equation (5) during cloudy conditions (the revised definition of w_T^{*3} already includes surface-based entrainment), and only the first term in clear conditions. These modifications alter the PBL top flux and hence the counter-gradient term (γ_c), though we, like Wilson (2015), note the effect of this change is miniscule. While the buoyancy flux generated due to longwave radiative cooling rarely exceeds 4 $m^2\ s^{-3}$ for the DYCOMS RF01 ocean case, over land strong thermals generated by the surface flux causes buoyancy fluxes to regularly exceed 10 $m^2\ s^{-3}$ (Figures 1a and 1b, later). For the ocean cases, the thermals are not as strong as for the land case and we do not need to enhance the counter-gradient term further to account for them: the boundary layer becomes sufficiently well mixed upon addition of the cloud top driven mixing profile. For the remainder of the study, we refer to the corrected YSU scheme as YSU-BUOY.

2.2.2. ACM2

2.2.2.1. ACM2: Model Description

The ACM2 uses a staggered grid where scalar quantities and horizontal momentum components are represented at the grid layer centers designated by i, while the vertical fluxes, vertical velocities, and eddy diffusivities are located at the layer interface $i+1/2$. Hence, ACM2 computes flux at the interface as

$$\left(\left[\overline{w'c'}\right]_{i+1/2}\right)_{ACM2} = -(1-f_{conv})K_{C,z_{i+\frac{1}{2}}}\frac{\partial C_i}{\partial z} + f_{conv}\frac{K_{C,z=\frac{3}{2}}}{\Delta z_{z=\frac{3}{2}}}\frac{(h-z_{i+1/2})}{(h-z_{3/2})}\ (C_1-C_i), \tag{9}$$

where f_{conv} is a weighting factor that splits mixing between local and nonlocal components and is expressed as

$$f_{conv} = \left[1+\frac{\kappa^{-2/3}}{0.1a}\left(-\frac{h}{L}\right)^{-1/3}\right]^{-1}, \tag{10}$$

where a is a constant set to 7.2, h is the PBL height, and L is the Obukhov length. The value of f_{conv} for stable and neutral conditions is 0 (local transport only) and increases to a maximum of about 0.5 in strongly convective conditions (splitting mixing between local and nonlocal components; Pleim, 2007).

2.2.2.2. Proposed Modifications: ACM2-BUOY

ACM2 was designed such that the second term on the right-hand side of equation (9) represents mass fluxes due to upward transport in convectively buoyant plumes. The first term on the right-hand side of equation (9) represents the local eddy diffusion similar to the first term in equation (1) for the YSU scheme. Thus, to account for longwave cooling at the cloud top we utilize equations (5) and (6) to define $K_{C,z}$ in the same way as in YSU-BUOY. Similar to the YSU parameterization, we do not need to add in equation (9) an analogous term to the counter-gradient term in equation (9) because the longwave-cooling-driven downward thermals are not as strong as the upward thermals.

Initial testing revealed that the revised eddy diffusivity did not resolve PBL thermodynamic biases suggesting an underestimation of entrainment. Thus, a supplementary explicit entrainment scheme was implemented only for cloudy conditions in the same way as in YSU-BUOY (equation (3)), except with $A=0.08$. The smaller value of A here is due to the existing ability of ACM2 to implicitly model entrainment.

The ACM2 modifications proposed here are only intended to test the hypothesis that entrainment flux is being underestimated—they are not intended for operational use, as the explicit entrainment scheme conflicts with the original design of ACM2. The experimental ACM2 scheme will be referred to as ACM2-BUOY.

2.2.3. MYNN

The MYNN scheme determines the eddy diffusion coefficient as a function of turbulent kinetic energy (TKE, $q^2=\overline{u'^2+v'^2+w'^2}$), stability correction functions for momentum (S_M, used, e.g., wind) and heat (S_H, used, e.g., heat and moisture), and the master length scale (L) as

$$\left(\overline{w'c'}\right)_{MYNN} = -qLS_{M,H}\frac{\partial C}{\partial z}. \tag{11}$$

The master length scale is a function of the Obukhov length, TKE, and buoyancy flux (Nakanishi & Niino, 2004). However, despite the fact that MYNN uses a more complex TKE closure framework, we find that MYNN is not capable of accurately representing the vigorous vertical mixing throughout the STBL, as well as the heating and drying due to entrainment mixing of dry air aloft. This could be a result of inadequate representation of longwave radiative cooling and/or inadequate modeling of cloud top entrainment. In this

regard, the TKE equation currently employed in MYNN is lacking in accounting for STBL-specific processes. Due to the complexity of MYNN, further modification was left for future work. The unmodified MYNN results are provided for reference only.

2.3. Corrections to the Inversion Height Determination in the Single-Column Model

In WRF v3.7.1, the YSU and ACM2 schemes detect planetary boundary layer height (inversion height) based on the height at which the bulk Richardson number (Ri_b) exceeds 0 for YSU and 0.25 for ACM2. In ACM2, Ri_b is computed as a function of virtual potential temperature θ_v, while the recent addition of the top-down mixing option in YSU (Wilson, 2015) revised the computation of Ri_b to a function of ice-liquid potential temperature θ_{li}. MYNN uses a hybrid method which blends PBL heights determined from (1) the first point at which θ_v exceeds the minimum θ_v within the PBL by 1.5 K in neutral and convective conditions and (2) where TKE drops below 5% of the maximum TKE near the surface in stable conditions (Benjamin et al., 2016).

As θ_v is defined for unsaturated air, θ_v is not conserved within the cloud layer (θ_v increases with height above the cloud base height). Therefore, ACM2 and MYNN, (and YSU prior to the top-down mixing option, where the conserved variable θ_{li} was introduced) underestimate inversion height (Figure 2). False assignment of the PBL height to a lower level within the boundary layer could lead to underestimation of thermodynamic jump values and hence entrainment in YSU, YSU-BUOY, and ACM2-BUOY, as well as an underestimation of eddy viscosity near the PBL top in YSU and YSU-BUOY.

Therefore, PBL height diagnostics need to be corrected before the proposed parameterizations can be tested. To this end, we substitute θ_v in all computations regarding PBL height in ACM2 and MYNN with liquid virtual potential temperature $\theta_{vl}=\theta_l(1+0.608q_t)$ which is conserved within the STBL (Grenier & Bretherton, 2001).

Theoretically, cloud top height coincides with the inversion base height z_{inv}; however, even after correcting the inversion height detection this may not always be true. Therefore, in equations (6–8) where the existence of a cloud impacts mathematical terms, the cloud top height z_{ctop} is substituted for z_{inv}, where cloud top height z_{ctop} is defined as the highest grid level with liquid water content in the SCM within 1 grid point of z_{inv}. LES inversion height is defined at the maximum gradient of liquid potential temperature.

2.4. Correction of SCM Numerical Instability

As of WRF v3.7.1, the function which calculates temperature and scalar tendencies in the SCM computes vertical derivatives using a two-point second-order accurate centered finite difference with uniform spacing centered on the boundary between two grid points. This scheme was found to produce a numerical instability at the inversion layer which acts to unphysically transport moisture from the dry air aloft into the moister air within the PBL, as well as lock adjacent grid cells to the same thermodynamic values, and the effects increased with simulation time. The cause appears to be numerical dispersion caused by the strong temperature and moisture gradients near the inversion. The finite differencing scheme was modified to a five-point fourth-order accurate centered finite difference scheme with uneven spacing (Bowen & Smith, 2005) relative to the grid center (as is customary in NWPs, the simulations in this study were performed with nonuniform grid spacing), and the numerical instability was partially alleviated. Locking no longer occurs except for in 1–2 grid points above the inversion for MYNN at the end of the 24 h simulation, and the drying of above PBL q_t is limited to 0.5 g/kg, compared to 0.9 g/kg originally (removing almost all water vapor present). Because the function in question is specific to the SCM, this numerical instability does not affect real-data WRF simulations. In the SCM, this numerical instability does not affect the entrainment velocity, but rather increases the moisture jump value, so that entrainment drying $\left(\overline{w'q_t'}\right)_{z_{inv}}=w_e\Delta q_{t_{z_{inv}}}$ is overestimated; however, this effect is small.

3. Evaluation of WRF SCM Simulations of the STBL

3.1. Baseline DYCOMS RF01 Ocean Case Evaluation

The diurnal cycle of the WRF SCM vertically integrated LWP is shown in Figure 3, along with LES results. Both ACM2 and MYNN yield a LWP that is more than twice that in LES, while YSU (with the Wilson, 2015 addition of top-down diffusion) matches well with LES. For ACM2 and MYNN, the LWP increases rapidly at initialization at midnight reaching a maximum LWP shortly after sunrise after which LWP decreases during

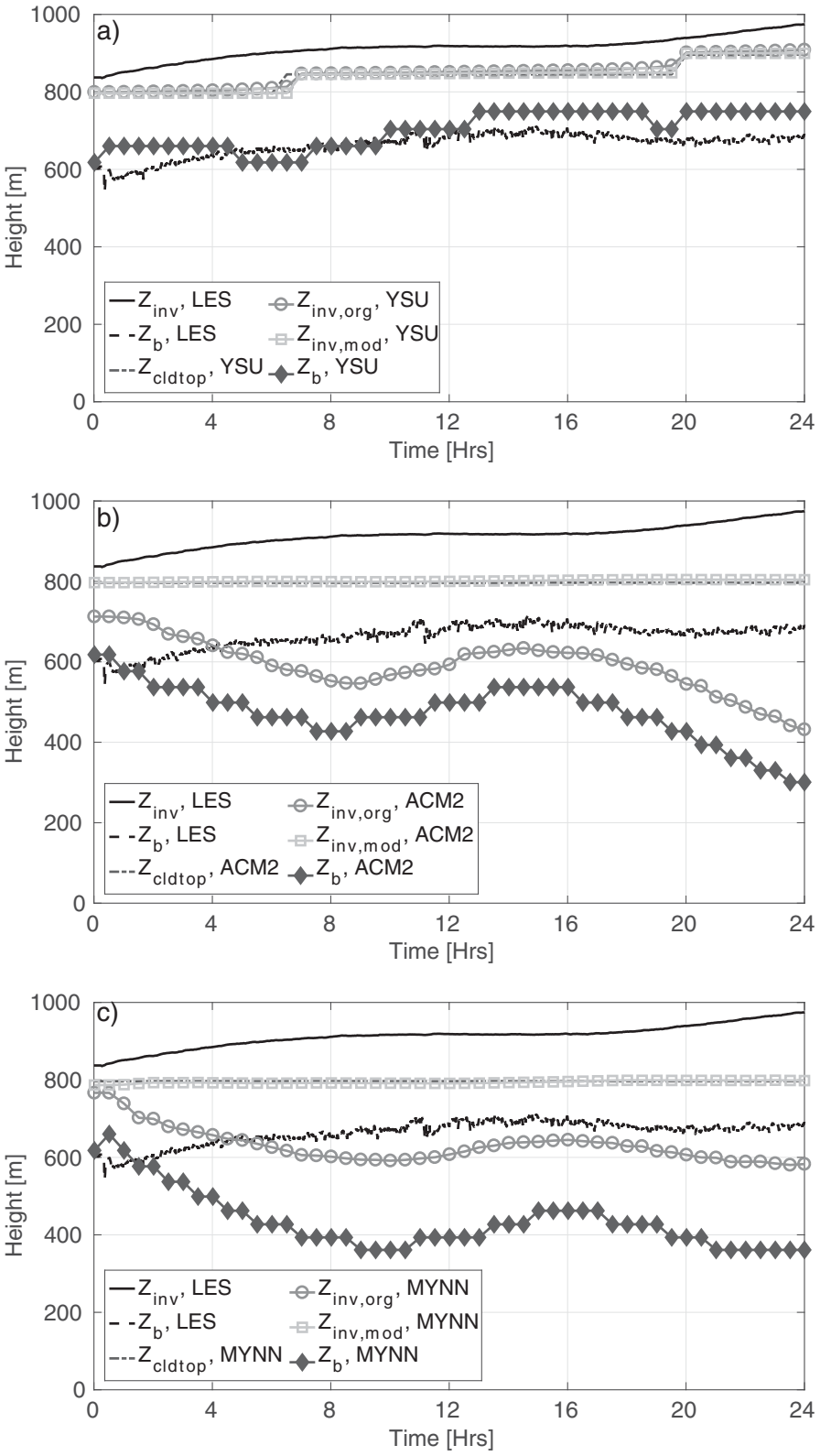

Figure 2. Inversion heights as detected by the original SCM algorithm ($z_{inv,org}$) plotted with grey lines and circle markers and inversion heights as detected by the modified SCM algorithm plotted with grey lines and square markers for (a) YSU scheme, (b) ACM2 scheme, and (c) MYNN scheme. LES derived inversion height is plotted with the solid black line. Cloud base heights are also shown for reference.

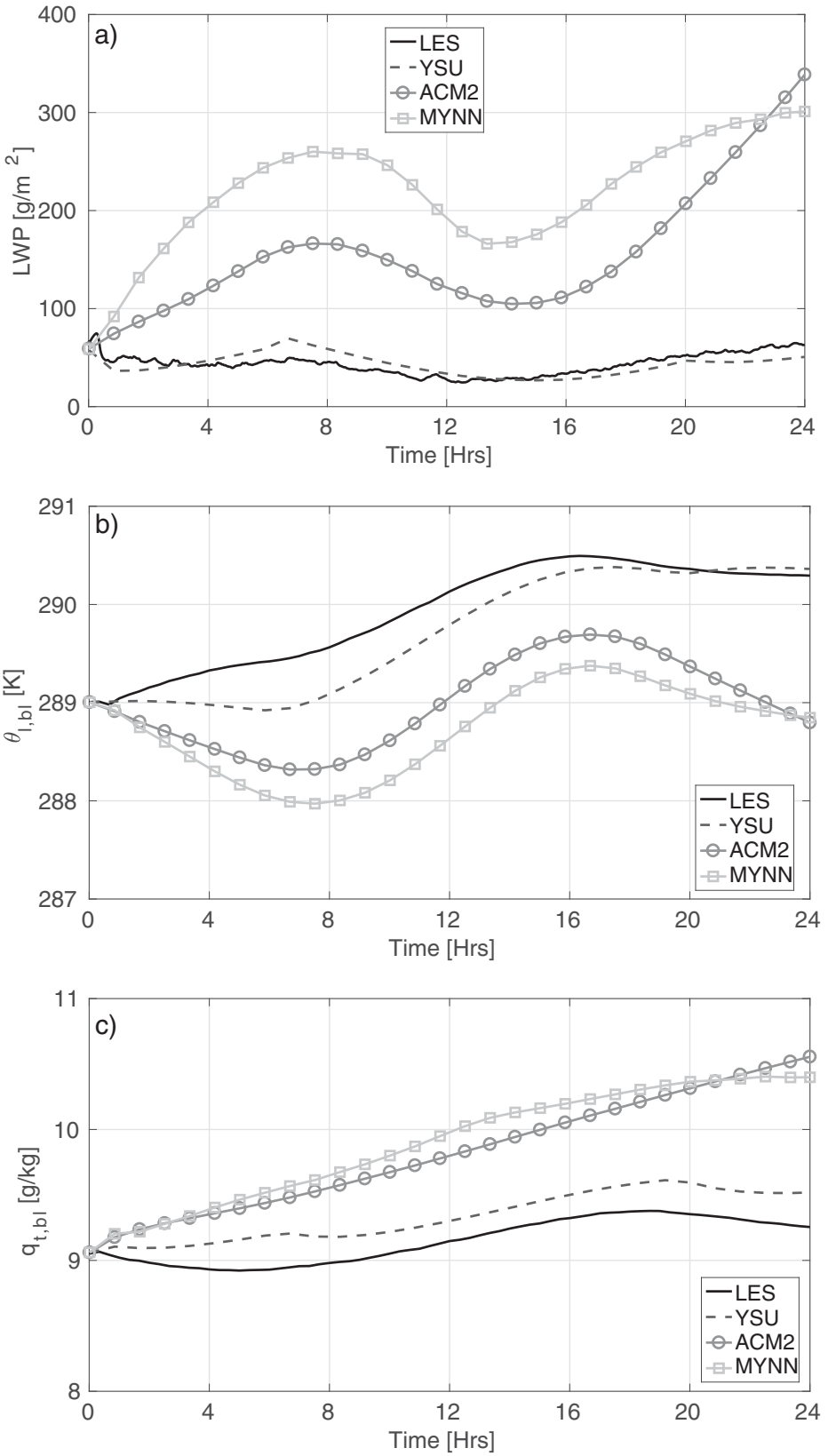

Figure 3. (a) Domain averaged vertically integrated LWP. (b) Boundary layer averaged liquid potential temperature and (c) total water mixing ratio.

the day due to solar heating and precipitation. Running YSU without the Wilson (2015) correction (not shown) yields similar results to those from ACM2 and MYNN.

Figure 3b depicts the boundary layer averaged liquid potential temperature, $\theta_l = \theta - \frac{L_v}{c_p} q_l$, with θ the potential temperature, L_v the latent heat for condensation of water, c_p the specific heat of dry air at constant pressure and q_l the cloud liquid water mixing ratio. The total water mixing ratio, $q_t = q_v + q_l$, which is the sum of water vapor (q_v) and cloud liquid water mixing ratio is plotted in Figure 3c. Both θ_l and q_t are conserved in adiabatic motions of moist air parcels in a well-mixed STBL (i.e., both variables are constant with height in the STBL); hence, we use the boundary layer averaged quantities as a proxy for the STBL heat and moisture content. All three schemes simulate lower θ_l and higher q_t values within the boundary layer compared to LES. Hence, the SCM yields a cooler, moister STBL. STBL moisture content simulated by the SCM increases throughout the 24 h simulation period. Since the surface flux is kept constant for both the LES and the SCM, the moisture and heat bias of the SCM compared to LES is indicative of deficiencies in either the microphysics or the PBL parameterizations.

3.2. Microphysics Scheme Evaluation

Table 2 outlines the different microphysics schemes employed in the study. For the YSU scheme, there is negligible dependence of LWP on the microphysics scheme (not shown). For the ACM2 and MYNN scheme, we observe a large spread in LWP for the different microphysics schemes, whereby the WSM5 scheme produces the least LWP (Figures 4a and 4b). The spread is mainly due to precipitation (Figure 5), whereby the different autoconversion schemes within the microphysics schemes form raindrops due to collision of cloud droplets at different efficiencies. The MYNN in particular experiences a strong growth in LWP initially, resulting in thicker clouds that drizzle more (Figure 4). The thick drizzling clouds simulated by the ACM2 and MYNN and different microphysics schemes are not consistent with DYCOMS LES results or the campaign measurements.

All microphysics schemes simulate the sharp increase in LWP at the start of the simulation; hence, the cold, moist bias of the PBL schemes is not a result of deficiencies in the parameterization of the microphysics schemes. Thus, we hypothesize that the overestimation of cloud liquid water content is the result of incorrect PBL parameterization of entrainment flux.

3.3. PBL Scheme Evaluation

In a one-dimensional PBL and neglecting horizontal advection and nonlocal terms, the tendency of a variable C, where C can represent θ_l or q_t, can be expressed in terms of the convergence of its flux F_c as

$$\frac{\partial C_{BL}}{\partial t} = -\frac{\partial F_c}{\partial z}, \tag{12}$$

where F_c can represent vertical turbulent (e.g., $\overline{w'c'}$) or radiative flux. The boundary layer average C_{BL} is used to facilitate analysis through a mixed layer framework, wherein the vertical gradient of F_c is linear and can be determined solely from the surface and PBL top fluxes. This formulation is sufficient to describe the tendency of C_{BL}, as mixing is assumed to occur instantaneously throughout the PBL. We use cloud thickness tendency as a proxy for the liquid water path tendency as they are analogues (Ghonima et al., 2015). The tendency is expressed as function of the inversion height z_{inv} and cloud base height z_b tendencies as $\frac{\partial h}{\partial t} = \frac{\partial z_i}{\partial t} - \frac{\partial z_b}{\partial t}$. For a well-mixed STBL, the cloud base height (z_b) tendency equation is expressed as

$$\frac{\partial z_b}{\partial t} = B_1 \frac{\partial \theta_{l,BL}}{\partial t} + B_2 \frac{\partial q_{t,BL}}{\partial t} + B_1 \frac{\partial F_R}{\partial z}, \tag{13}$$

where $B_1 = \partial z_b / \partial \theta_l$ and $B_2 = \partial z_b / \partial q_t$ (for full derivation, see Ghonima et al., 2015), and F_R is the sum of longwave and shortwave radiative fluxes. Since the inversion height change over the diurnal cycle is much smaller than that of the cloud base height (Figure 2), we will limit our analysis to the cloud base height tendency.

All three schemes produce a negative cloud base height tendency $\partial z_b / \partial t$, ranging from -5 to -15 mm s^{-1} nocturnally that is indicative of a thickening cloud layer (Figure 6a); during the day, solar loading causes the cloud to thin and hence $\partial z_b / \partial t$ to turn positive. The LES, on the other hand, simulates a cloud base height tendency that is initially slightly positive (slightly thinning) nocturnally and then near zero during the day before turning negative after sunset.

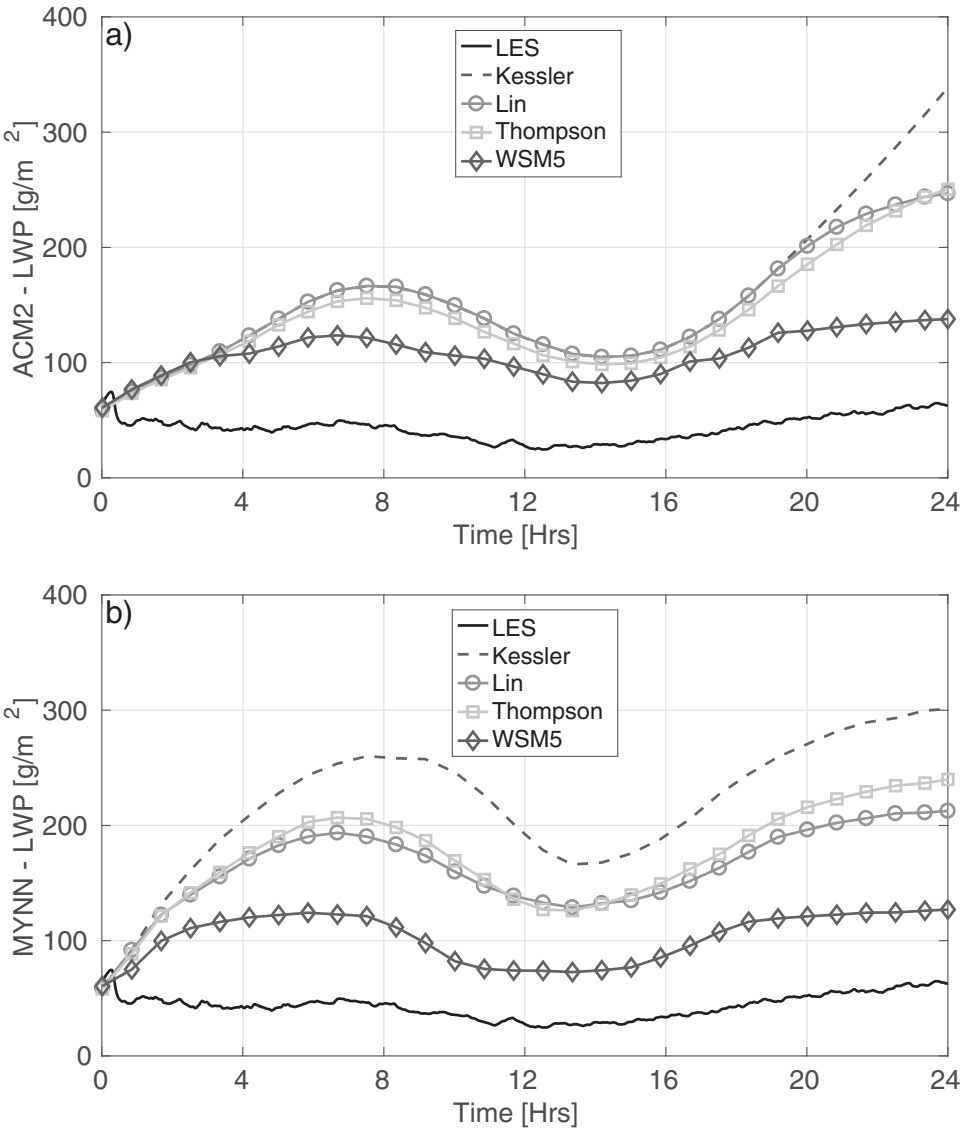

Figure 4. Domain averaged vertically integrated LWP in the DYCOMS RF01 test case for (a) ACM2 and (b) MYNN with different microphysics schemes (Table 2). Since the YSU showed negligible spread in LWP for all microphysics schemes, YSU is not shown.

Next, we substitute equation (12) into each term in equation (13) to split up the cloud base height tendency contributions integrated over the PBL due to liquid potential temperature vertical flux ($B_1\partial\overline{w'\theta_l'}/\partial z$), total water mixing ratio vertical flux ($B_2\partial\overline{w'q_t'}/\partial z$), and radiative flux ($B_1\partial F_R/\partial z$). Surface sensible heat flux and cloud top entrainment flux both act to warm the STBL, while surface latent heat flux acts to moisten the STBL and entrainment flux acts to dry the STBL. For the first 6 h, $B_1\partial\overline{w'\theta_l'}/\partial z$ is underestimated for all three schemes compared to the LES results, particularly for the MYNN (Figure 6b). During the day, $B_1\partial\overline{w'\theta_l'}/\partial z$ is then overestimated. Noting that the surface flux is held constant for all schemes and assuming the STBL is well mixed, we conclude that the entrainment flux warming is underestimated in the morning and evening in the three PBL schemes resulting in a cooler STBL with a thicker cloud deck.

Similarly, $B_2\partial\overline{w'q_t'}/\partial z$ is negative for the three PBL schemes, which indicates that there is little entrainment flux drying of the STBL. Therefore the surface latent heat flux moistening of the STBL dominates entrainment drying, thereby decreasing the cloud base height (Figure 6a). Thus, for all three schemes we observe a systematic underprediction of cloud top entrainment flux in the morning. Since the LES radiative scheme

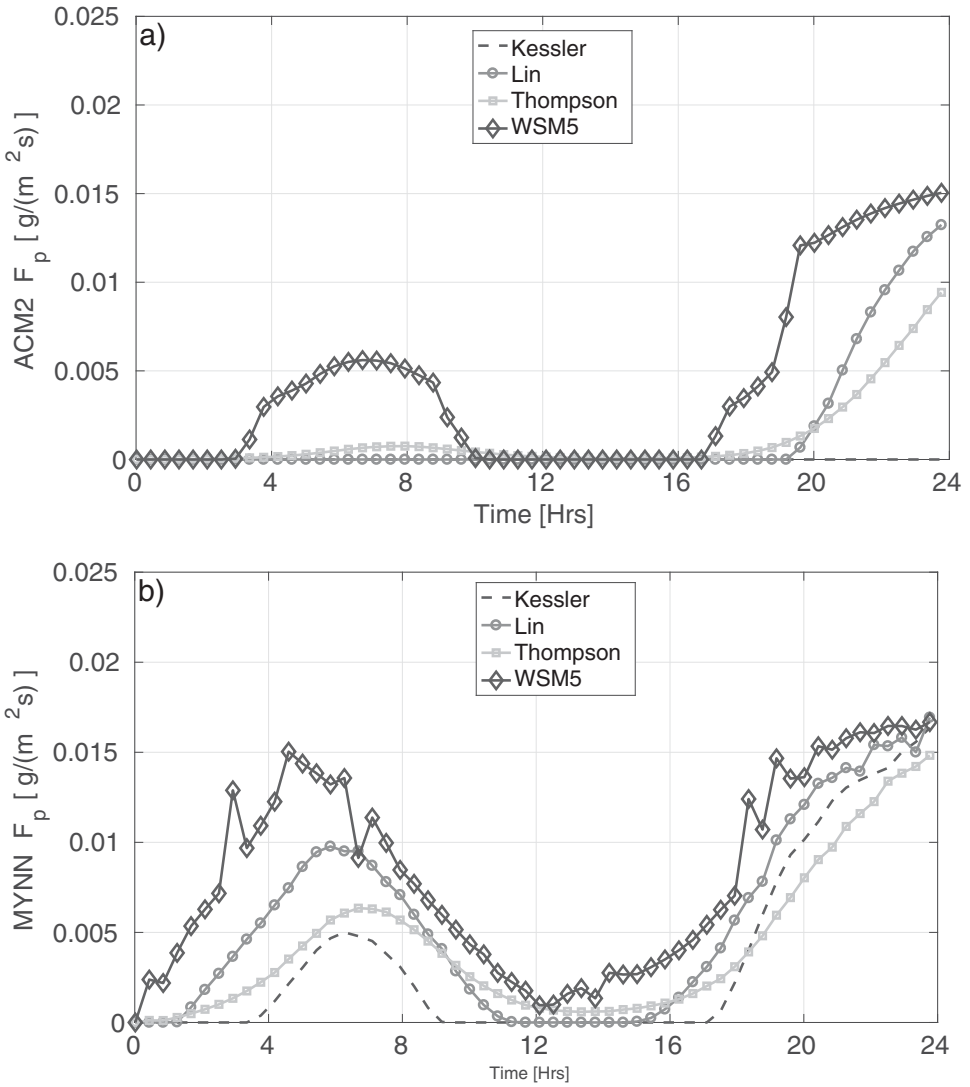

Figure 5. Precipitation flux at the surface for (a) ACM2 and (b) MYNN with different microphysics schemes. Since precipitation in the YSU scheme was 0 for all microphysics schemes, YSU is not shown.

simulates very similar radiative flux divergence to the SCM (Figure 6d), radiation does not appear to be the cause of discrepancy.

3.4. Modified PBL Scheme Validation

In this section, we validate the corrected PBL schemes for the DYCOMS RF01 case as well as the CGILS S12 control case. Results from MYNN will no longer be considered, as its complexity causes modification to exceed the scope of this paper. Furthermore, to test different regimes, we simulate STBL occurring over coastal lands where the main source of turbulence shifts from longwave cooling at the cloud top to surface-driven buoyancy flux during the day. Following Ghonima et al. (2016), we initialize the LES with DYCOMS profiles to a simplified land surface model that computes the surface flux based on prescribed Bowen ratio (defined as the ratio of sensible to latent heat flux) and net radiation at the surface. Root-mean-square errors (RMSE) and mean bias errors (MBE) for all simulations are given in Table 3.

3.4.1. DYCOMS RF01 Over Ocean

Both the corrected YSU scheme (YSU-BUOY) and experimental ACM2 scheme (ACM2-BUOY) simulate a drier warmer STBL that matches well with the LES (Figure 7), with ACM2 showing a dramatic improvement while YSU-BUOY performs similarly to YSU. This improvement is a result of increased entrainment flux drying and warming in the STBL in ACM2-BUOY (Figure 6). As expected, both schemes then simulate LWP close to the

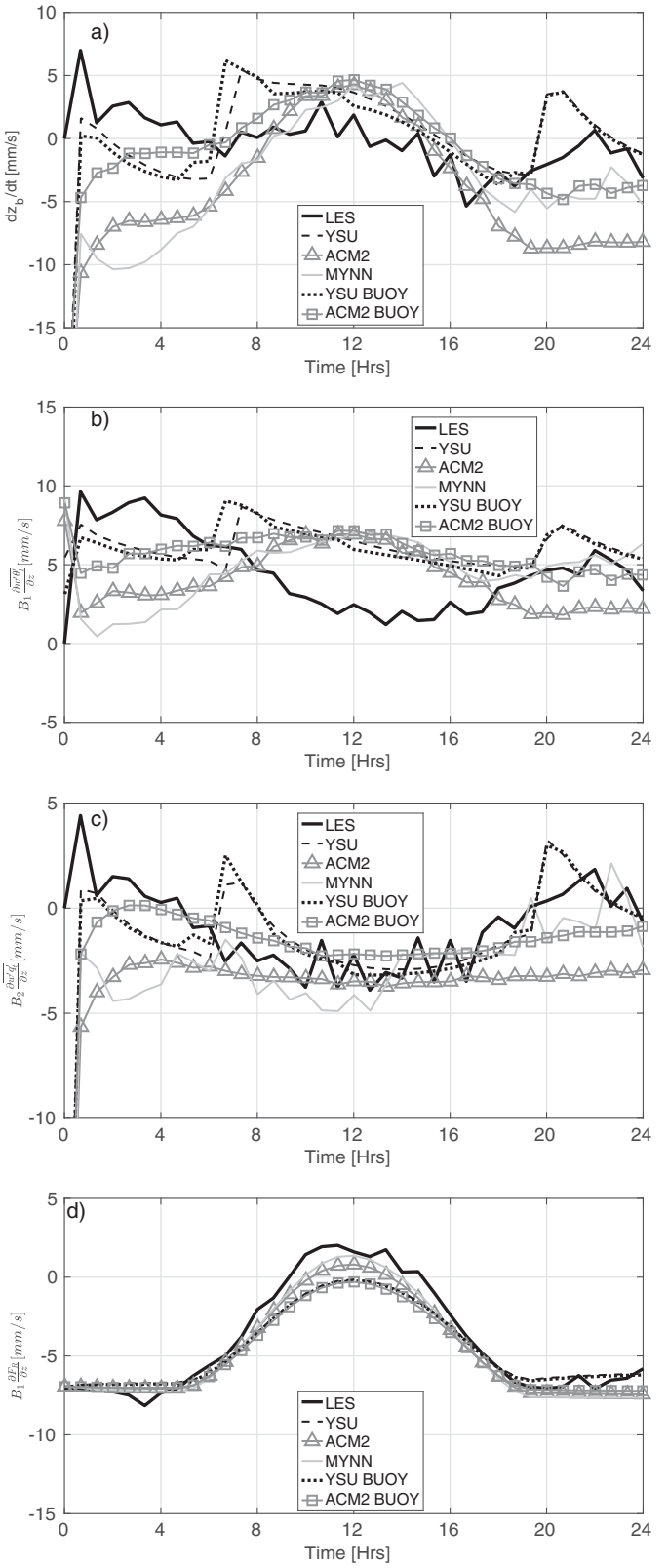

Figure 6. (a) Total cloud base height tendency, (b) θ_l vertical turbulent flux contribution to cloud base height tendency, (c) q_t vertical turbulent flux contribution to cloud base height tendency, and (d) radiative flux contribution to cloud base height tendency in the DYCOMS RF01 ocean case.

Table 3
Table of LWP Errors in (g/m^2) for Each Simulation Case and Each PBL Scheme

		YSU	YSU-BUOY	ACM2	ACM2-BUOY	MYNN
DYCOMS RF01 ocean	RMSE	10.5	9.9	123.9	13.8	184.2
	MBE	−0.6	−4.8	110.5	7.3	176.5
Wet land β=0.1	RMSE	40.9	28.0	91.2	20.9	117.1
	MBE	20.2	16.7	68.1	−2.0	101.7
Dry land β=1.0	RMSE	9.5	8.2	10.3	5.8	42.7
	MBE	−5.1	−3.3	6.6	1.0	25.0
CGILS S12 control ocean	RMSE	6.6	6.3	22.0	22.9	77.1
	MBE	−3.1	−0.5	8.2	−20.8	67.8

Note. Errors were computed over the full 24 h of simulation time.

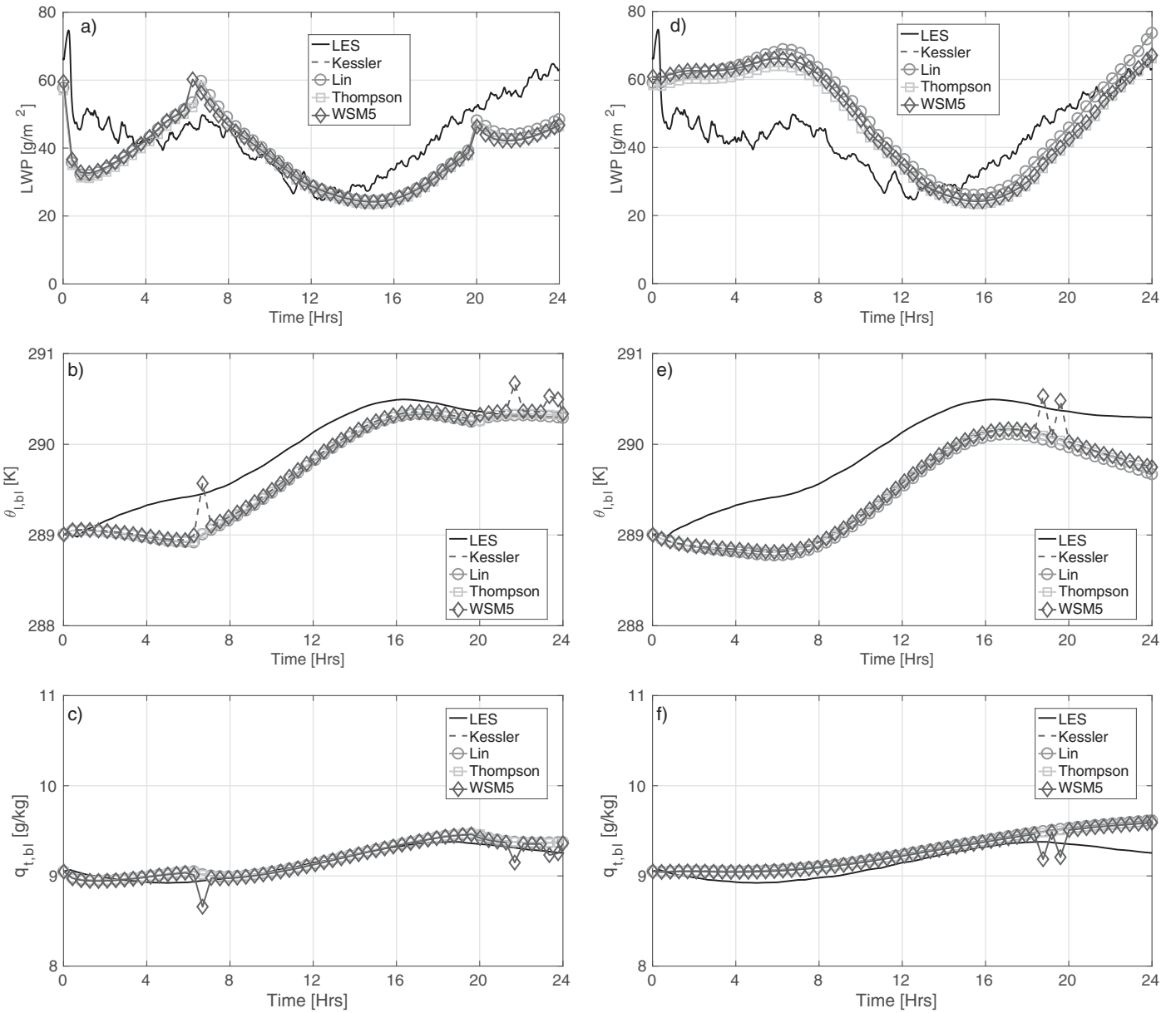

Figure 7. DYCOMS RF01 over ocean results for (top) domain averaged vertically integrated LWP, (middle) boundary layer averaged liquid potential temperature, and (bottom) total water mixing ratio. (a–c) YSU-BUOY and (d–f) ACM2-BUOY. See Figure 3 for comparison with unmodified schemes.

LES and DYCOMS measurements (Figure 7 and Table 3). We do not observe any dependence on the microphysics schemes as the reduced LWP eliminates precipitation in both schemes (not shown). While YSU-BUOY slightly underestimates LWP the diurnal cycle of LWP is accurately captured. Similarly, ACM2-BUOY accurately captures the diurnal cycle of LWP, though LWP is overestimated in the morning and underestimated in the evening.

3.4.1.1. Sensitivity to Vertical Resolution

Next, we test the effect of resolution on the YSU-BUOY scheme to find that resolution plays an important role (Figure 8). Instead of the 74 vertical levels employed for the other simulations, we ran YSU-BUOY with 50 vertical levels in the same configuration as the Rapid Refresh (RAP) mesoscale model and find that the LWP is less accurate, with larger LWP RMSE by 45% on average compared to the 74 vertical level simulation (RMSE and MBE are 11.8 and 14.3 g/m^2, respectively). The worse performance is mainly attributed to the coarse resolution at the inversion: the grid spacing at the temperature inversion in the RAP configuration is about 200 m, in contrast to about 50 m for the original 74 vertical levels. These increased errors are due not only to the decrease in grid points but also to the distribution of grid points within the boundary layer: in the original setup, 49 points are concentrated below 2 km, whereas only 14 points are below 2 km in the

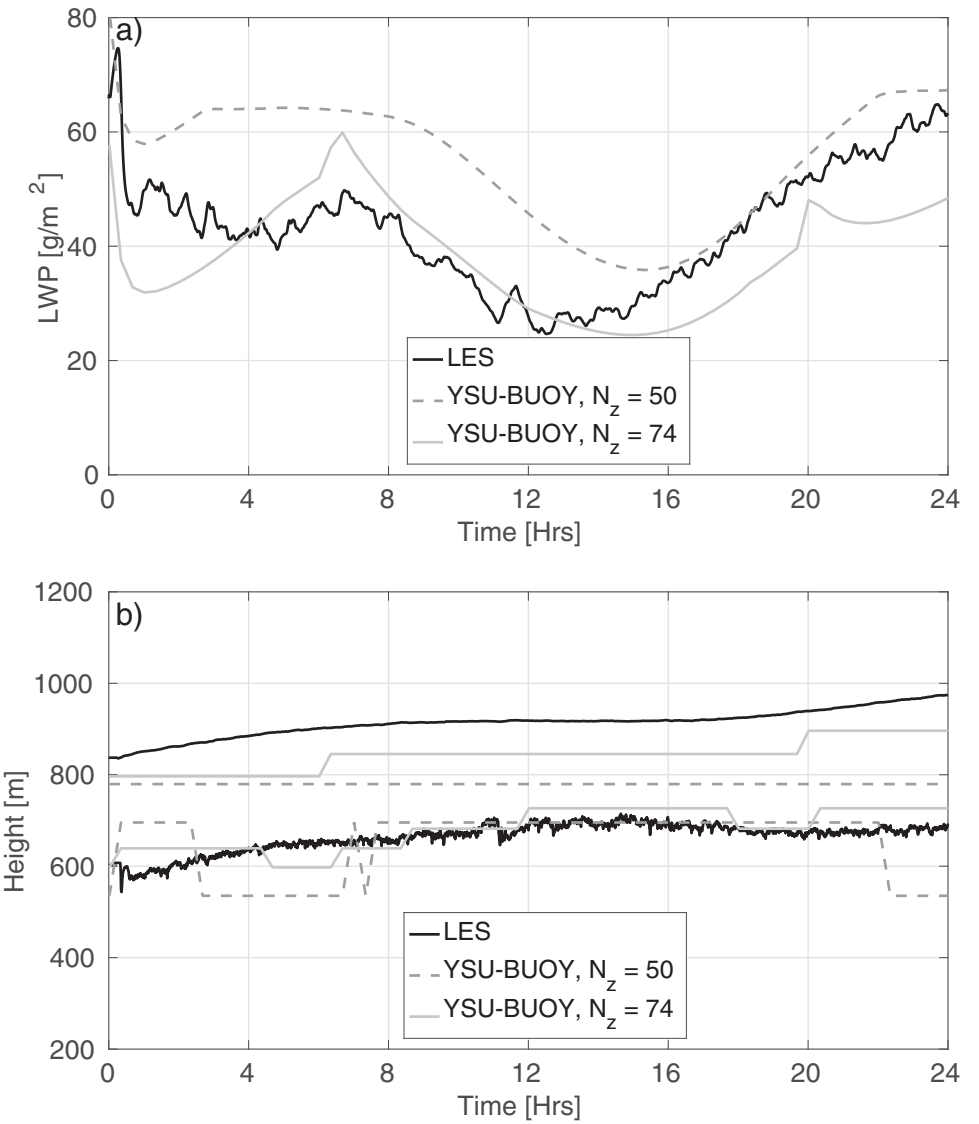

Figure 8. (a) Domain averaged vertically integrated LWP and (b) inversion height and cloud base height for LES (solid black line), YSU-BUOY with 50 vertical points (grey dashed line), and YSU-BUOY with 74 vertical points (grey solid line).

RAP configuration. The coarse resolution is unable to resolve the sharp gradients present at the temperature inversion, and the explicit entrainment parameterizations used here are sensitive to the thermodynamic jump values across the inversion (e.g., equation (3)). Additionally, the entrainment efficiency $A=a_1(1+a_2E)$ is dependent on the jump values through the evaporative enhancement term E, and the coefficient of E is $a_1a_2=4$ in the original YSU and 12 in YSU-BUOY. In the $N_z=74$ case, $0.7 < A < 0.9$, while in the $N_z=50$ case, $0.55 < A < 0.75$, leading to less entrainment and larger LWP in the coarse simulation. Similar sensitivity tests to vertical for the original YSU (not shown) showed that values of A were more stable at about 0.35. Due to this stability, LWP in YSU was more consistent between simulations, with the $N_z=50$ case (RMSE and MBE of 9.97 and 2 g/m^2) showing only 5% less LWP RMSE than the $N_z=74$ case (RMSE and MBE of 10.46 and -1.12 g/m^2). The use of more sophisticated inversion detection algorithms like those of Grenier and Bretherton (2001) may alleviate the dependence of inversion jump values on vertical resolution. Finer grid spacing near the temperature inversion also allows more granular PBL height changes rather than large jumps of several hundred meters at a time which leads to smoother thermodynamic jump time series. The improvement in the representation of STBL at the higher resolution could also be due to numerics—for instance, Lenderink et al. (2004) found that convective schemes tend to produce liquid water through a numerical detrainment process at the cloud top.

3.4.2. Wet Land ($\beta=0.1$)

To demonstrate performance of the scheme in different conditions following Ghonima et al. (2016), we test YSU-BUOY and ACM-BUOY for STBL occurring over coastal lands with DYCOMS initial profiles. The land differs from the ocean because of the diurnal cycle of surface latent and sensible heat fluxes. The Bowen ratio controls the ratio of sensible and latent heat fluxes and therefore the rate of heating and moistening of the STBL. We find that for a wet land surface ($\beta=0.1$) YSU-BUOY is able to simulate LWP similar to LES for the first 12 h of the simulation capturing the increase in inversion height driven by surface flux during the day (Figures 9a and 9b). However, after 12 h as surface flux decreases, the convective velocity scale and hence surface-driven mixing also decrease. Additionally, the clouds are not thick enough to produce sufficient longwave-induced turbulent mixing in the boundary layer. Due to the lower simulated turbulent mixing overall, YSU-BUOY underestimates entrainment, leading to cooler, moister STBL with higher LWP compared to the LES. Compared with the unmodified YSU, YSU-BUOY more accurately simulates inversion height, boundary layer temperature, and hence LWP for most of the simulation. For hours 12–17 in the simulation,

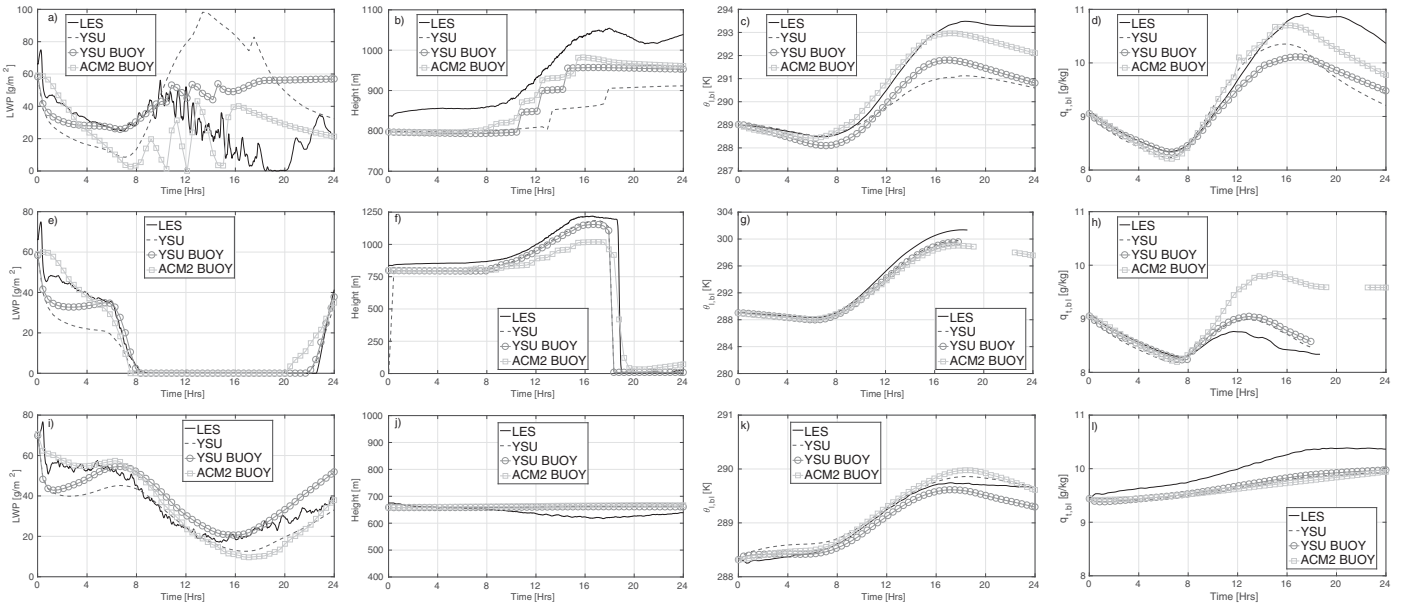

Figure 9. Comparison between LES (solid), YSU (dashed black), YSU-BUOY (grey circles), and ACM2-BUOY (grey squares) for (a, e, i) LWP, (b, f, j) inversion height, (c, e. k) liquid potential temperature of the boundary layer ($\theta_{l,bl}$), and (d, f, l) total water mixing ratio ($q_{t,bl}$), for the wet land case with Bowen ratio equal 0.1 (Figures 9a–9d), dry land case with Bowen ratio equal 1.0 (Figures 9e–9h), CGILS S12 control ocean case (Figures 9i–9l). Boundary layer averages were not computed for times with zero inversion height.

YSU-BUOY underpredicts boundary layer moisture compared with YSU, indicating excessive entrainment drying, though the reverse is true afterward.

ACM2-BUOY appears to overestimate entrainment for this case, suggesting the supplemental entrainment was too strong. Furthermore, the cloud unphysically dissipates twice, coinciding with times when the PBL height increases. As the temperature inversion rises, the inversion jump values between adjacent grid cells approaches zero, causing an excessive estimation of the entrainment velocity w_e (recall from equation (5) that $\Delta\theta_v$ appears in the denominator). After 12 h, ACM2-BUOY also appears to underestimate entrainment.

3.4.3. Dry Land (β=1.0)

Over a relatively dry land surface (β=1.0), YSU-BUOY accurately simulates the cloud dissipation driven by surface sensible heat flux warming. Furthermore, YSU-BUOY is able to capture the sharp increase in inversion height in the dry convective boundary layer regime during the day and the subsequent collapse at night (Figures 9e–9h). ACM2-BUOY performs similarly well here for both dissipation time and boundary layer heating but underestimates PBL height and overestimates boundary layer moisture.

3.4.4. CGILS S12 Control Over Ocean

In order to test how well YSU-BUOY and ACM2-BUOY perform under different initial conditions, we compare both schemes to LES for the CGILS S12 control case. Both YSU-BUOY and ACM2-BUOY match the results of the LES relatively well, simulating shortwave daytime radiative warming (not shown) and the resulting drop in LWP (Figures 9i–9l).

4. Conclusions

We employed three WRF-SCM simulations with various PBL schemes and benchmarked the results against LES to investigate the capability of the YSU, ACM2, and MYNN PBL schemes in modeling the STBL. We find that ACM2 and MYNN underestimate entrainment flux resulting in a cooler, moister boundary layer with much larger LWP. The ACM2 scheme's turbulent flux parameterization does not take into account the longwave-cooling-induced turbulence in the boundary layer, thereby leading to entrainment underestimation. The MYNN TKE closure scheme fails in representing the STBL which indicates the inherent difficulty in modeling such regimes and a deficiency in the current TKE equation. Although the YSU scheme performs well for ocean cases, simulations over land showed room for improvement. The choice of microphysics schemes primarily regulates the upper bound of LWP through different amounts of drizzle precipitation, but an unphysical initial sharp rise in LWP is common in all microphysics schemes. This rise in LWP further substantiates that entrainment flux is insufficient to counteract the longwave radiative cooling of the STBL and surface latent heat flux moistening. In order to improve the parameterization of the STBL we propose a revision to the YSU scheme (YSU-BUOY) that accounts for the skewness of top-driven convection and parameterizes entrainment based on the in-cloud buoyancy flux rather than radiative flux divergence as in the Wilson (2015) YSU update. This revision results in a more robust entrainment model since longwave emission becomes insensitive to changes in LWP for thick clouds (Kazil et al., 2015). Similar modifications were made to the ACM2 scheme (ACM2-BUOY) in order to explore the impact of explicitly modeling these effects.

We tested both YSU-BUOY and ACM2-BUOY against LES for four different test cases and find that more accurate entrainment fluxes result in LWPs that closely match those simulated by the LES. The improvement of YSU-BUOY over the original YSU scheme is predominantly due to the revision of the convective velocity scale. In ACM2-BUOY, the improvement is mostly due to the addition of the explicit entrainment model. However, because the ACM2-BUOY scheme is capable of implicitly modeling some entrainment, the contribution from both entrainment models is difficult to modulate. In addition, ACM2-BUOY currently suffers from discretization issues, preventing immediate implementation.

While Wilson (2015) was interested in simulation of fog, fog and STBL share many similarities. Our original YSU-BUOY model development actually preceded the publication of the Wilson article and was originally published in Ghonima et al. (2016). We therefore arrived independently at the same conclusion regarding deficiencies in current PBL parameterizations: a lack of accounting for downward mixing originating from the cloud top driven by longwave cooling and inaccurate modeling of entrainment mixing across the cloud top interface.

Modeling of mixing driven by longwave cooling at the cloud top increases the coupling between the cloud and land/ocean surface, leading to more realistically well-mixed STBL; this enhanced mixing may reduce the occurrence of stratocumulus breakup due to boundary layer decoupling, wherein cool, moist air is unable to mix into the cloud deck. The fluxes of heat and moisture caused by entrainment are more difficult to determine, as these entrainment fluxes depend not only on the entrainment velocity w_e (which is itself difficult to determine) but also on the inversion jump values ΔC_i. While the improvements in STBL simulations shown here under a variety of conditions are encouraging, the remaining biases in boundary layer heat and moisture suggest further research is needed. Hence, entrainment remains the subject of active ongoing research, though this study shows a step toward correctly simulating STBL in WRF. Future work will explore modifications aimed at improving the modeling of STBL processes in MYNN and include extensive testing of these modified schemes in the full 3-D WRF, both in idealized and real scenarios. Proper validation will then aid the implementation of these modifications into WRF.

Correctly modeling entrainment under conditions typical to NWPs and GCMs (i.e., coarse discretization of thermodynamic gradients, especially vertically, and limited information available both in time and space) is expected to improve predictions of boundary layer temperature, humidity, and precipitation for the weather forecasting community, ceiling heights for the aviation industry, and cloud cover for the solar energy and climate modeling communities. In this study, the most accurate modeling of cloud top entrainment was achieved with an explicit entrainment model utilizing a revised convective velocity scale, which is a function of in-cloud buoyancy flux rather than radiative flux divergence, thereby eliminating insensitivity for thick clouds.

Acknowledgments
The authors express their gratitude to the South Coast Air Quality Management District for funding under contract number 15650. All data for this paper are properly cited and referred to in the reference list. The source code for the LES model used in this study, the UCLA-LES, is freely available at https://github.com/uclales, and initial profiles and forcings are included. The WRF model is also freely available at http://www2.mmm.ucar.edu/wrf/users/downloads.html. Mohamed S. Ghonima and Handa Yang contributed equally to this work.

References

Ackerman, A. S., vanZanten, M. C., Stevens, B., Savic-Jovcic, V., Bretherton, C. S., Chlon, A., . . . Zulauf, M. (2009). Large-eddy simulations of a drizzling, stratocumulus-topped marine boundary layer. *Monthly Weather Review*, *137*, 1083–1110. https://doi.org/10.1175/2008MWR2582.1

Benjamin, S. G., Weygandt, S. S., Brown, J. M., Hu, M., Alexander, C. R., Smirnova, T. G., . . . Kenyon, J. S. (2016). A North American hourly assimilation and model forecast cycle: The Rapid Refresh. *Monthly Weather Review*, *144*(4), 1669–1694.

Blossey, P. N., Bretherton, C. S., Zhang, M., Cheng, A., Endo, S., Heus, T., . . . Xu, K. M. (2013). Marine low cloud sensitivity to an idealized climate change: The CGILS LES intercomparison. *Journal of Advances in Modeling Earth Systems*, *5*, 234–258. https://doi.org/10.1002/jame.20025

Bowen, M. K., & Smith, R. (2005). Derivative formulae and errors for non-uniformly spaced points. *Proceedings of the Royal Society of London A: Mathematical, Physical and Engineering Sciences*, *461*(2059), 1975–1997.

Chou, M.-D., & Suarez, M. J. (1999). *A solar radiation parameterization for atmospheric studies* (NASA Tech. Rep. NASA/TM-1999–10460, Vol. 15, 38 pp.). Washington, DC: NASA.

Chou, M.-D., & Suarez, M. J. (2001). *A thermal infrared radiation parameterization for atmospheric studies* (Rep. NASA/TM-2001–104606, Vol. 19, 55 pp.). Washington, DC: NASA.

Ghonima, M. S., Heus, T., Norris, J. R., & Kleissl, J. (2016). Factors controlling stratocumulus cloud lifetime over coastal land. *Journal of the Atmospheric Sciences*, *73*(8), 2961–2983.

Ghonima, M. S., Norris, J. R., Heus, T., & Kleissl, J. (2015). Reconciling and validating the cloud thickness and liquid water path tendencies proposed by R. Wood and J. J. van der Dussen et al. *Journal of the Atmospheric Sciences*, *72*, 2033–2040. https://doi.org/10.1175/JAS-D-14-0287.1

Grenier, H., & Bretherton, C. S. (2001). A moist PBL parameterization for large-scale models and its application to subtropical cloud-topped marine boundary layers. *Monthly Weather Review*, *129*, 357–377. https://doi.org/10.1175/1520-0493(2001)129<0357:AMPPFL>2.0.CO;2

Hahn, C. H., & Warren, S. G. (2007). *A gridded climatology of clouds over land (1971–96) and ocean (1954–97) from surface observations worldwide* (Numeric Data Product NDP-026E). Oak Ridge, TN: Carbon Dioxide Information Analysis Center, Oak Ridge National Laboratory.

Hartmann, D. L., & Short, D. A. (1980). On the use of earth radiation budget statistics for studies of clouds and climate. *Journal of the Atmospheric Sciences*, *37*, 1233–1250. https://doi.org/10.1175/1520-0469(1980)037<1233:OTUOER>2.0.CO;2

Hong, S.-Y., Dudhia, J., & Chen, S.-H. (2004). A revised approach to ice microphysical processes for the bulk parameterization of clouds and precipitation. *Monthly Weather Review*, *132*, 103–120. https://doi.org/10.1175/1520-0493(2004)132<0103:ARATIM>2.0.CO;2

Hong, S.-Y., Noh, Y., & Dudhia, J. (2006). A new vertical diffusion package with an explicit treatment of entrainment processes. *Monthly Weather Review*, *134*, 2318–2341. https://doi.org/10.1175/MWR3199.1

Kazil, J., Feingold, G., & Yamaguchi, T. (2015). Wind speed response of marine non-precipitating stratocumulus clouds over a diurnal cycle in cloud-system resolving simulations. *Atmospheric Chemistry and Physics Discussions*, *15*, 28395–28452. https://doi.org/10.5194/acpd-15-28395-2015

Kessler, E. (1969). On the distribution and continuity of water substance in atmospheric circulations. In *On the distribution and continuity of water substance in atmospheric circulations* (pp. 1–84). Boston, MA: American Meteorological Society.

Lenderink, G., Siebesma, A. P., Cheinet, S., Irons, S., Jones, C. G., Marquet, P., . . . Soares, P. M. M. (2004). The diurnal cycle of shallow cumulus clouds over land: A single-column model intercomparison study. *Quarterly Journal of the Royal Meteorological Society*, *130*(604), 3339–3364.

Lin, Y.-L., Farley, R. D., & Orville, H. D. (1983). Bulk parameterization of the snow field in a cloud model. *Journal of Applied Meteorology and Climatology*, *22*, 1065–1092. https://doi.org/10.1175/1520-0450(1983)022<1065:BPOTSF>2.0.CO;2

Lock, A. P., Brown, A. R., Bush, M. R., Martin, G. M., & Smith, R. N. B. (2000). A new boundary layer mixing scheme. Part I: Scheme description and single-column model tests. *Monthly Weather Review*, *128*(9), 3187–3199.

Lock, A. P., & Macvean, M. K. (1999). The parametrization of entrainment driven by surface heating and cloud-top cooling. *Quarterly Journal of the Royal Meteorological Society*, *125*, 271–299. https://doi.org/10.1002/qj.49712555315

Moeng, C.-H. (2000). Entrainment rate, cloud fraction, and liquid water path of PBL stratocumulus clouds. *Journal of the Atmospheric Sciences*, *57*, 3627–3643.

Nakanishi, M., & Niino, H. (2004). An improved Mellor–Yamada level-3 model with condensation physics: Its design and verification. *Boundary Layer Meteorology*, *112*, 1–31. https://doi.org/10.1023/B:BOUN.0000020164.04146.98

Nakanishi, M., & Niino, H. (2009). Development of an improved turbulence closure model for the atmospheric boundary layer. *Journal of the Meteorological Society of Japan, Series II*, *87*(5), 895–912.

Nicholls, S., & Turton, J. D. (1986). An observational study of the structure of stratiform cloud sheets: Part II. Entrainment. *Quarterly Journal of the Royal Meteorological Society*, *112*(472), 461–480.

Paulson, C. A. (1970). The mathematical representation of wind speed and temperature profiles in the unstable atmospheric surface layer. *Journal of Applied Meteorology*, *9*(6), 857–861.

Pincus, R., & Stevens, B. (2009). Monte Carlo spectral integration: A consistent approximation for radiative transfer in large eddy simulations. *Journal of Advances in Modeling Earth Systems*, *1*, 1. https://doi.org/10.3894/JAMES.2009.1.1

Pleim, J. E. (2007). A combined local and nonlocal closure model for the atmospheric boundary layer. Part I: Model description and testing. *Journal of Applied Meteorology and Climatology*, *46*, 1383–1395. https://doi.org/10.1175/JAM2539.1

Randall, D. A., Coakley, J. A., Lenschow, D. H., Fairall, C. W., & Kropfli, R. A. (1984). Outlook for research on subtropical marine stratification clouds. *Bulletin of the American Meteorological Society*, *65*, 1290–1301. https://doi.org/10.1175/1520-0477(1984)065<1290:OFROSM>2.0.CO;2

Skamarock, W. C., Klemp, J. B., Dudhia, J., Gill, D. O., Barker, D. M., Duda, M. G., . . . Powers, J. G. (2008). *A description of the advanced research WRF version 3* (NCAR Tech. Note NCAR/TN 475+STR). Boulder, CO: National Center for Atmospheric Research.

Stevens, B. (2002). Entrainment in stratocumulus-topped mixed layers. *Quarterly Journal of the Royal Meteorological Society*, *128*(586), 2663–2690.

Stevens, B. (2010). Cloud-top entrainment instability? *Journal of Fluid Mechanics*, *660*, 1. https://doi.org/10.1017/S0022112010003575

Stevens, B., Moeng, C.-H., Ackerman, A. S., Bretherton, C. S., Chlond, A., de Roode, S., . . . Zhu, P. (2005). Evaluation of large-eddy simulations via observations of nocturnal marine stratocumulus. *Monthly Weather Review*, *133*, 1443–1462. https://doi.org/10.1175/MWR2930.1

Thompson, G., Field, P. R., Rasmussen, R. M., & Hall, W. D. (2008). Explicit forecasts of winter precipitation using an improved bulk microphysics scheme. Part II: Implementation of a new snow parameterization. *Monthly Weather Review*, *136*, 5095–5115. https://doi.org/10.1175/2008MWR2387.1

Wilson, T. H. (2015). *The evolution and life cycle of valley cold pools*. Los Angeles, CA: University of California, Los Angeles. Retrieved from http://escholarship.org/uc/item/44c4k8gh

Zhang, M., Bretherton, C. S., Blossey, P. N., Austin, P. H., Bacmeister, J. T., Bony, S., . . . Zhao, M. (2013). CGILS: Results from the first phase of an international project to understand the physical mechanisms of low cloud feedbacks in single column models. *Journal of Advances in Modeling Earth Systems*, *5*, 826–842. https://doi.org/10.1002/2013MS000246

Zhang, M., Bretherton, C. S., Blossey, P. N., Bony, S., Brient, F., & Golaz, J.-C. (2012). The CGILS experimental design to investigate low cloud feedbacks in general circulation models by using single-column and large-eddy simulation models. *Journal of Advances in Modeling Earth Systems*, *4*, M12001. https://doi.org/10.1029/2012MS000182

Zhu, P., Bretherton, C. S., Köhler, M., Cheng, A., Chlond, A., Geng, Q., . . . Stevens, B. (2005). Intercomparison and Interpretation of single-column model simulations of a nocturnal stratocumulus-topped marine boundary layer. *Monthly Weather Review*, *133*, 2741–2758. https://doi.org/10.1175/MWR2997.1